Cellular Physiology and Biochemistry

Cell Physiol Biochem 2013;32(suppl 1):146-156
DOI: 10.1159/000356634
Published online: December 18, 2013
Accepted: November 27, 2013

1421-9778/13/0327-0146$38.00/0

Original Paper

Surface-Enhanced Raman Spectroscopy (SERS) Tracking of Chelerythrine, a Na^+/K^+ Pump Inhibitor, into Cytosol and Plasma Membrane Fractions of Human Lens Epithelial Cell Cultures

Kevin M. Dorney[a] Ioana E.P. Sizemore[a] Tariq Alqahtani[b,c] Norma C. Adragna[b,c] Peter K. Lauf[b,c,d]

[a]Departments of Chemistry, [b]Pharmacology & Toxicology, [c]Cell Biophysics Group, and [d]Pathology, Wright State University, Dayton, OH, USA

Key Words
Chelerythrine • Human Lens Epithelia • Surface-Enhanced Raman Spectroscopy • Cellular Distribution • Na^+/K^+ Pump

Abstract
Background/Aims: The quaternary benzo-phenanthridine alkaloid (QBA) chelerythrine (CET) is a pro-apoptotic drug and Na^+/K^+ pump (NKP) inhibitor in human lens epithelial cells (HLECs). In order to obtain further insight into the mechanism of NKP inhibition by CET, its sub-cellular distribution was quantified in cytosolic and membrane fractions of HLEC cultures by surface-enhanced Raman spectroscopy (SERS). ***Methods:*** Silver nanoparticles (AgNPs) prepared by the Creighton method were concentrated, and size-selected using a one-step tangential flow filtration approach. HLECs cultures were exposed to 50 µM CET in 300 mOsM phosphate-buffered NaCl for 30 min. A variety of cytosolic extracts, crude and purified membranes, prepared in lysing solutions in the presence and absence of a non-ionic detergent, were incubated with AgNPs and subjected to SERS analysis. Determinations of CET were based on a linear calibration plot of the integrated CET SERS intensity at its 659 cm^{-1} marker band as a function of CET concentration. ***Results:*** SERS detected chemically unaltered CET in both cytosol and plasma membrane fractions. Normalized for protein, the CET content was some 100 fold higher in the crude and purified plasma membrane fraction than in the soluble cytosolic extract. The total free CET concentration in the cytosol, free of membranes or containing detergent-solubilized membrane material, approached that of the incubation medium of HLECs. ***Conclusion:*** Given a negative membrane potential of HLECs the

Peter K. Lauf, M.D. Professor

The Cell Biophysics Group, Depts. of Pathology, and of Pharmacology and Toxicology
Wright State University, Boonshoft School of Medicine, Dayton, OH 45459 (USA)
Tel. +1 937-775-2889, Fax + 1 937-775-7221, E-Mail peter.lauf@wright.edu

data suggest, but do not prove, that CET may traverse the plasma membrane as a positively charged monomer (CET^+) accumulating near or above passive equilibrium distribution. These findings may contribute to a recently proposed hypothesis that CET binds to and inhibits the NKP through its cytosolic aspect.

Introduction

Chelerythrine (CET) is a quaternary benzo-phenanthridine alkaloid (QBA) of 348 Daltons mass and extracted from *Papaveraceae*, i.e. plants of the Poppy family. In solutions near physiological pH, CET is positively charged (CET^+) due to an iminium group (N^+=C) attracting small anions such as Cl. At increased pH values, CET^+ loses its charge and becomes a pseudobase with an apparent pK_a value of ~9 [1] . In the past, QBAs such as CET and its sister alkaloids, the sanguinarines, have been widely used as medicinal remedies in insecticides, bactericides, fungicides, viricides, in ointments, mouthwash solutions, and tooth pastes, sedatives and anti-helmintics [2]. More recently, CET had been first reported as a protein kinase C (PKC) inhibitor [3] and, utilizing this mechanism, later heralded as a potential anti-cancer agent capable of inducing apoptosis in a variety of cancer cell lines [4-6]. Acting as a BH3-mimetic, CET induces apoptosis by binding to BH1-like motifs of B cell lymphoma type 2 (Bcl-2) proteins inhibiting pro-survival B-cell lymphoma extra large (BclXI) proteins and activating mitochondrial Bcl-2 associated X (Bax)/ B*cl-2 homologous antagonist-killer (BAK) protein* pro-apoptotic mechanisms [7-9].

Recently, CET was shown to inhibit ouabain-sensitive K^+ or Na^+/K^+ pump (NKP) influx in human lens epithelial cells (HLECs) without interference with ouabain binding and PKC-mediated NKP phosphorylation [10]. The CET structure-related sanguinarines have been known for a long time to inhibit the NKP in a variety of tissue preparations [11-17], without an explanation for this effect. Sequence homologies between BH1-like motifs originally reported to bind CET in Bcl-Xl proteins and found in the cytoplasmic aspect of the crystal structure of the NKP led to the hypothesis that CET may inhibit the NKP function through these BH1 motifs [10]. The amino acid sequence ARAAEILARDGPN of the first putative CET binding site resides in the A domain of the NKP and has two arginine (R) residues. Interestingly, fluorescence studies suggest interaction of R residues with sanguinarines, however, in the carboxy (C)-terminus of the NKP [18]. Moreover, sequence homologies of the NKP BH1-like motifs found in all P-type ATPases suggest other cellular metabolic pathways can be influenced by the presence of CET [10].

Although QBAs have been shown to rapidly diffuse across plasma membranes and may be used as fluorescing DNA probes [19], the mechanism of transmembrane distribution of CET is unknown and thus the question as to whether the charged monomeric CET^+ or its lipid soluble pseudobase traverse the plasma membrane prior to binding and affecting intracellular structures such as the NKP remains unresolved. Traditional techniques for monitoring the amount and localization of active metabolites in biological systems (*i.e.,* ultraviolet-visible absorption spectrophotometry, fluorescence spectroscopy, liquid chromatography, etc.) are often limited by low detection limits, increased experimental duration and cost, or indirect observation of the species of interest via a (radio) chemical "label". Recently, surface-enhanced Raman spectroscopy (SERS) has emerged as a powerful molecular sensing technique due to its high degree of molecular specificity, low detection limits, and multiplex detection capabilities [20, 21], permitting accurate determination of distribution and amount of metabolites in biological systems with very short experimental durations, a *conditio sine qua non* for pharmacological studies.

In order to obtain insight into the interaction of CET with the NKP, this study attempts to track the distribution of CET across the plasma membrane into the cytosol of HLECs, our model, in which CET was shown to inhibit the NKP [10]. Raman analysis of a stock CET solution exhibited a few very weak peaks; however, upon the addition of silver nano-particles (AgNPs), a large signal enhancement was observed yielding vibration-rich spectra.

The SERS enhancement of CET facilitated the construction of a calibration function for determination of the concentration of monomeric CET in the cytosol and its content in membrane particulate fractions. The alkaloid CET accumulated in the cytosol and plasma membranes at concentrations near or above diffusion equilibrium suggesting transport as an organic cation CET^+, presumably the species interacting with Bcl-2 proteins and NKP [10].

Materials and Methods

Reagents

Silver nitrate (99.5%, $AgNO_3$), sodium borohydride (99%, $NaBH_4$), were purchased from Fisher Scientific (Fairlawn, NJ) and chelerythrine chloride (98%, CET) from Acros Organics (Fairlawn, NJ). Potassium bromide (≥ 99%, KBr) and nitric acid (Optima grade) were purchased from Fisher Scientific. All reagents were utilized without further purification. High quality water (> 18 MΩ cm) was obtained from a LabConco water purification system and utilized as solvent throughout. Cell culture media and buffers were described earlier [10]. The NKP Na^+-conformational buffer consisted of the following reagents (in mM, all from Sigma Chemical, St. Louis, MO): 100 NaCl, 20 KCl, 20 $MgCl_2$, 20 Imidazole, 1 NaF, and HALT (Pierce Biochemicals) as protease inhibitor.

Cell Culture and Preparation of Cytosol and Membrane Extracts

HLECs were obtained as a primary fetal human lens cell line (FHL124) by courtesy of Dr. John Reddan, Oakland University, Michigan, and were cultured and propagated using specialty support and media as described earlier by this laboratory [10, 22, 23]. Cells were grown to near confluence in 100 mm diameter Petri dishes (49.1 cm^2 surface area/dish), culture media aspirated, washed twice with each 4 mL room temperature (RT)-equilibrated balanced salt solution (BSS), and exposed to 4 mL phosphate buffered saline (PBS) without or with 50 μM CET in the presence and absence of dimethylsulfoxide (DMSO) at 37 °C for 30 min, a time sufficient to nearly completely inhibit NKP [10]. Thereafter, cells were washed thrice with 4 mL ice-cold PBS, all supernatant fluids removed, and each dish covered with 0.4 mL M-PER® (Pierce Biochemicals) lysing solution containing 1:100 HALT reagent to stop proteolysis, and maintained for 10 min on a shaker at RT. Cellular debris was collected into Eppendorf tubes, which were then spun for 2 min at 14,000 g in an Eppendorf RT centrifuge to separate the cytosolic supernatants from the crude membrane particulate material. It was noted that the cytosol of the CET-treated cultures was slightly yellow, suggesting that CET had entered the cells. The crude membrane pellet was resuspended and washed 4 times in fresh M-PER® solution, after which the final pellet was dissolved in 0.5 mL M-PER® solution containing 1% 3-[(3-cholamidopropyl)dimethylammonio]-1-propanesulfonate (CHAPS), a non-ionic detergent known to solubilize membrane proteins by replacing membrane lipids. These final solubilized crude membrane samples were thrice ultra-sonicated on ice with 3 bursts to achieve maximal membrane disintegration. All samples were spun at 14,000 g for 2 min, the supernatant kept and the small finite pellet discarded. Aliquots of 0.05 mL supernatant were removed for protein analysis by the BIORAD® technique. Samples were stored at -20 °C for further SERS-based analysis.

In order to obtain a purified membrane preparation, HLECs, after CET exposure, were washed as described above, but then collected from the Petri dishes by scraping into a HALT-containing NKP Na^+-conformational buffer. The scrape was sonicated on ice as described above, and then centrifuged in a Beckman Optima XL ultracentrifuge (Beckman Co, Stanford Ca) at 4,600 g for 10 min at 4 °C to remove mitochondria and nuclear material followed by a final centrifugation at 131,000 g for 1 h at 4 °C to obtain the final plasma membrane pellet. This membrane pellet, further solubilized by sonication in NKP buffer containing 1% CHAPS and stored in aliquots at -80 °C, possesses only the α1 subunit of the NKP [10].

Estimation of Cell Volume and Calculation of Cytosolic Dilution

Based on previous estimates of endothelial and lens epithelial cell volume [23, 24] of 10^{-11} L/cell and an average cell count of 10^6/dish, a total cell volume of 10^{-2} mL/dish was estimated. As an example, given that 3 Petri dishes/control or experimental cells were available, which received a total M-PER lysing solution of 1.2 mL, the final total volume was 1.23 mL, *i.e.*, the dilution of the original cytoplasm was estimated to be 41 fold; and 71 in another experiment.

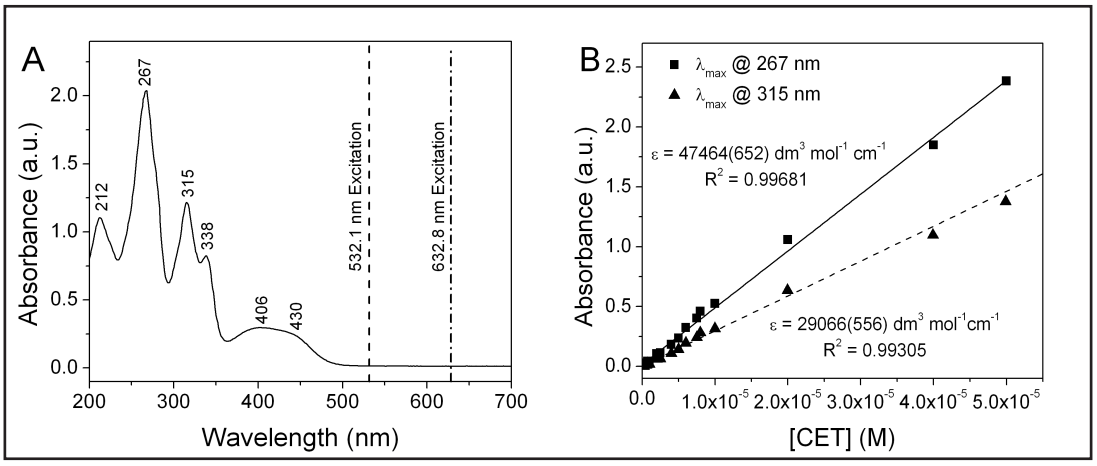

Fig. 1. A) UV-VIS absorption spectrum of monomeric CET solution (10^{-4} M). Dashed lines indicate the laser excitation wavelengths utilized in the SERS and Raman measurements, respectively. B) Plot of absorbance versus CET concentration along with linear fits to determine the extinction coefficients of the 267 nm and 315 nm absorbance bands in A. Uncertainties in the molar absorption coefficient *(ε)* are indicated parenthetically.

AgNP Synthesis, Size-Selection, and Concentration

AgNPs were synthesized in a batch-wise process via a modified Creighton method [25] employing the ice-cold reduction of $AgNO_3$ (1.0 mM, 50 mL) by $NaBH_4$ (2.0 mM, 300 mL). The formation of spherical AgNPs of moderate size distribution (~1-200 nm in diameter [26] was confirmed by the presence of an intense, symmetric ultraviolet-visible (UV-VIS) absorption peak at 392 nm. Once characterized, individual batches of AgNPs (350 mL each) were combined to achieve a total volume of 4.0 L. Tangential flow filtration [27] was then employed to size-select AgNPs, while eliminating the reaction byproducts/excess reagents and increasing the concentration of nanosilver for optimum SERS-based sensing. It was recently shown that the optimal size of AgNPs for SERS enhancements is ~50 nm in diameter[28]. Briefly, 4.0 L of colloid was recirculated through a hollow fiber polysulfone filter module (50 nm pore size, 390 cm^2 surface area, Spectrum Labs®) yielding a retentate of AgNPs of increased diameter (≥ 50 nm) and a filtrate containing dilute, smaller AgNPs (< 50 nm). The concentrated AgNPs (Ag_{50C}) were stored at ~ 4 °C until further use in SERS measurements.

Raman and SERS Measurements and Analysis

Raman and SERS measurements were conducted using a LabRamHR 800 system (Horiba Scientific, Inc.) coupled to either an internal HeNe laser (632.8 nm, 15 mW) or an external, frequency-doubled Nd:YAG laser (532.1 nm, 15 mW) with an acquisition time of 20 s and 3 s, respectively. The laser beam was focused into a 2 mL quartz cuvette carrying the Raman or SERS sample via a high stability, confocal microscope (BX 41) using a 50X objective. Serial dilutions of a CET stock solution (20 mM) were performed prior to the SERS analysis, yielding concentrations of 10^{-3} M through 10^{-9} M. Aliquots of the CET solutions were briefly incubated with the Ag_{50C} colloid, followed by addition of 1.0 M KBr to induce AgNP aggregation and SERS "hot-spot" formation [28] prior to analysis. SERS samples of HLEC extracts of the plasma membrane and cytosol were prepared in a similar fashion, and the total CET concentration in each extract was estimated via a standard calibration curve constructed from the SERS scattering intensities of the stock CET solutions. Peak integration routines and user-defined baseline correction algorithms were performed in Origin 8.5 software for each Raman and SERS spectrum.

Results

Raman and SERS Analysis of Monomeric CET

Prior to SERS analysis, the UV-VIS absorption spectrum of 10^{-4} M CET revealed absorption peaks at 212, 267, 315, 338 and 406-430 nm (Fig. 1A). The extinction spectrum

Table 1. Tentative Assignments of Aqueous Raman and SERS Vibrational Modes of CET[a,b,c]. [a]Mode designations: δ, scissoring; ν, stretching; ρ, rocking; σ, deformation; , ω, wagging; τ, torsion; i.p., in-plane; o.p., out-of-plane. [b]Intensity abbreviations: vw, very weak; w, weak; mw, medium-weak; m, medium; ms, medium-strong; s, strong. [c]Assignments derived from Ref [29-31]

Raman Vibrational Mode (cm^{-1})	Tentative Assignment	SERS Vibrational Mode (cm^{-1})	Tentative Assignment
435vw	o.p. τ(C-C-C) backbone	387w	o.p. σ(Aryl)
530vw	sextant σ(Aryl)	430ms	o.p. τ(C-C-C) backbone
668w	i.p. ν(C-C-C)	476w	Mixed o.p. σ(Aryl)
741vw	σ(dioxolene)	498w	
784w	mixed o.p. τ(CH)	527ms	o.p. sextant σ(Aryl)
832vw	adjacent ρ(CH)	577mw	o.p. τ(C-C-C) backbone
1161w	i.p. σ(Aryl)	**659s**	**i.p. ν(C-C-C)**
1239w	symmetric ν(Aryl-O)	707w	σ(dioxolene)
1291w	i.p. δ(C=C)+δ(N=C)	731w	
1346s		778ms	o.p. τ(CH)
1375ms	ν(C-C-C) of chrysene backbone	827w	adjacent ρ(CH)
1399s		972w	
1486mw	σ(Aryl-CH)	1046w	ν(Aryl-O-CH_2)
1507w	ν(Aryl-CH)	1096m	
1547m	ν(C=C)+ν(C=N)	1152w	σ(Aryl)
1582w	Quadrant ν(C=C) skeletal	1173w	τ(CH-N-CH_3)
		1233w	ν(C-C)
		1280mw	i.p. δ(C=C)+δ(N=C)
		1338m	ν(C-C-C) of chrysene backbone
		1367s	
		1390s	
		1474w	σ(Aryl-CH)
		1539w	ν(C=C)+ν(C-N)
		1572m	
		1596mw	Quadrant ν(C=C) skeletal
		1618w	ν(C=C)

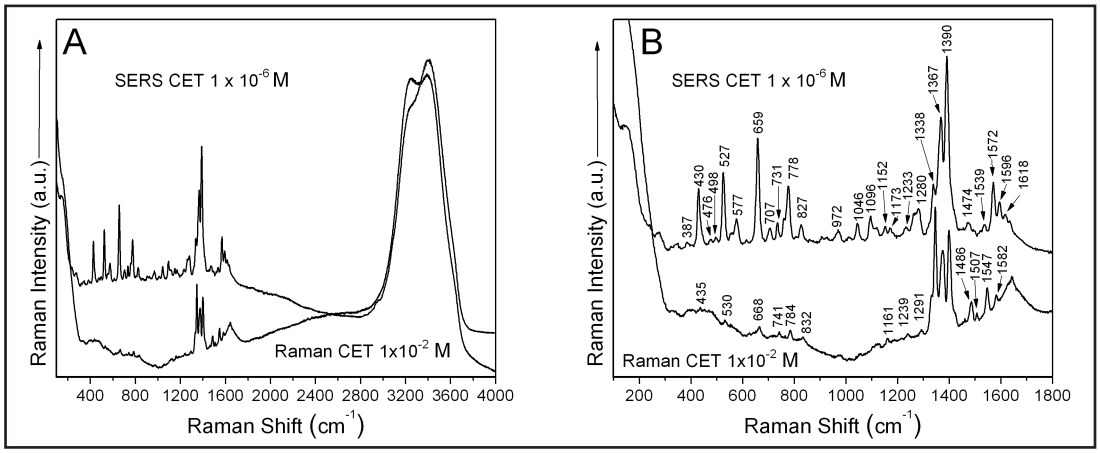

Fig. 2. A) Raman and SERS spectra of monomeric CET chloride solution at 10^{-2} M and 10^{-6} M, respectively. B) Expanded Raman and SERS spectra of CET in the 100-1800 cm^{-1} fingerprint region. Acquisition times were 30 s and 3 s for Raman and SERS measurements under 632.8 nm and 532.1 nm excitation, respectively. The SERS spectra in A and B are intensity-shifted for comparison.

as a function of CET concentration, along with the molar absorption coefficients calculated for the most prominent UV absorption peaks at 267 and 315 nm, not readily available in the literature, are given in Figure 1B.

CET contains a highly chromophoric imine bond, which experiences pre-resonance effects under 532 nm excitation and leads to a large fluorescent background in the Raman spectrum. However, the Raman spectrum of monomeric CET exhibited weak, yet distinctive

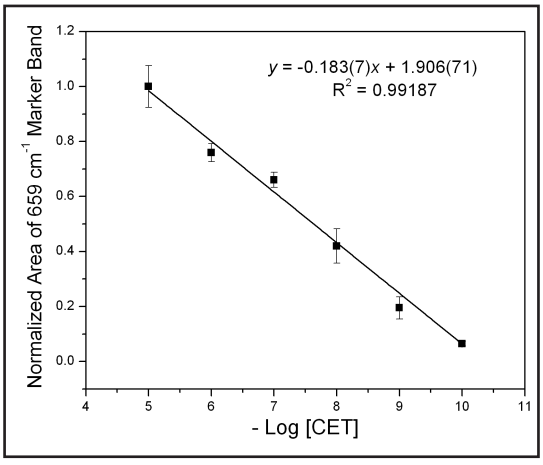

Fig. 3. Calibration plot relating the normalized 659 cm^{-1} peak area to the concentration of CET within each of the standard SERS samples. Error bars depict the standard deviation of three different CET solutions measured at each concentration. Error bars may be smaller than the symbols.

vibration modes upon excitation via the 632.8 nm HeNe laser (Fig. 2A). Characteristic functional group-vibration modes and those reported in the literature were utilized in order to provide a tentative assignment for each peak observed within the Raman spectrum (Table 1). Raman spectra of monomeric CET exhibited low signal-to-noise ratios for concentrations lower than 10^{-2} M, *i.e.*, far above the physiologically active concentrations of the monomer.

The addition of $AgNP_{50C}$ to stock solutions of CET not only yielded an exponential increase in scattering intensity, but also effectively quenched the fluorescence resulting from pre-resonance effects at concentrations as high as 10^{-4} M. The SERS spectra of monomeric CET showed a vibration-rich structure (Fig. 2B). In addition, the large increase in SERS signal observed for CET-$AgNP_{50C}$ mixtures yielded sub-picomolar detection limits (*i.e*, 10^{-10} M), which are well below IC_{50} values reported in the literature for diverse inhibitory functions by this drug. Vibration-rich SERS spectra (data not shown) were also observed for CET solutions containing the original unmodified AgNP colloid.

However, the SERS spectra using the modified Ag_{50C} exhibited greater spectral intensities, which is in good agreement with literature reports of SERS scattering as a function of AgNP size. SERS spectral analysis of vibration bands was performed in a similar manner as for the regular Raman scattering spectra (Table 1). It should be noted that the SERS analysis of CET has been sparsely reported and the assignments provided here serve only as tentative descriptors.

The four vibration modes occurring at 430 (o.p. τ(C-C-C)), 527 (o.p. sextant σAryl), 659 (in bold in Table 1, defining stretched (C-C-C) bonds) and 778 cm^{-1} (o.p. (CH)) were utilized as "marker bands" of CET (Table 1) due to the large spectral intensity and lack of overlap with adjacent peaks. Therefore, the presence of any one of these four marker bands in cellular extracts can confirm the presence of monomeric CET. In addition to determining several characteristic marker bands for spectral identification, the in-plane skeletal stretching mode at 659 cm^{-1} was observed to have the greatest intensity of all the marker bands and was thus utilized to quantify the concentration of CET in biological samples. The constructed calibration function revealed a linear relationship between the normalized 659 cm^{-1} peak areas and the concentration of the CET solutions from 10^{-5} M to 10^{-10} M (Fig. 3). Despite the presence of the four marker modes, accurate peak integration parameters could not be obtained for solutions greater than 10^{-5} M due to the increased fluorescence of free CET molecules.

Small aliquots of plasma membrane and cytosolic HLEC extracts (50 – 100 µL) were quantitatively diluted with either water (Raman) or the Ag_{50C} and KBr (SERS) to a total volume of 2 mL prior to spectral analysis. The normal Raman spectrum of the cytosolic extracts showed few, yet distinctive peaks corresponding to the DMSO solvent utilized in the extraction procedure (Figure 4A). A large fluorescent background was observed for the crude plasma membrane extract under normal Raman scattering conditions (*i.e.,* in the absence of AgNPs), thus obscuring all vibration modes aside from a lone DMSO peak at 679 cm^{-1}. No CET

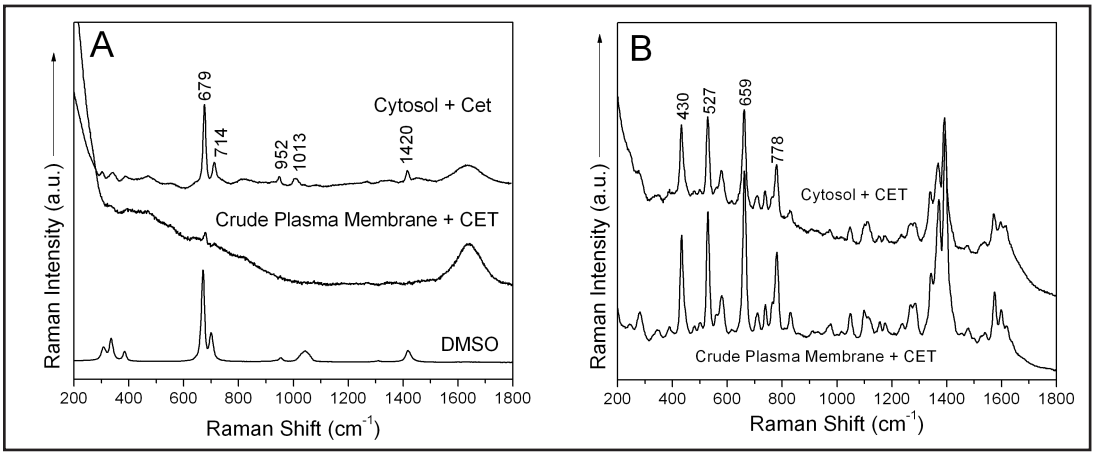

Fig. 4. A) Ordinary Raman spectra of cytosolic and crude plasma membrane extracts from LECs treated with CET in DMSO, collected using a 532.1 nm excitation line. B) SERS spectra of the same extracts in A, showing significant signal enhancement. Spectra in A and B are intensity-shifted for comparison.

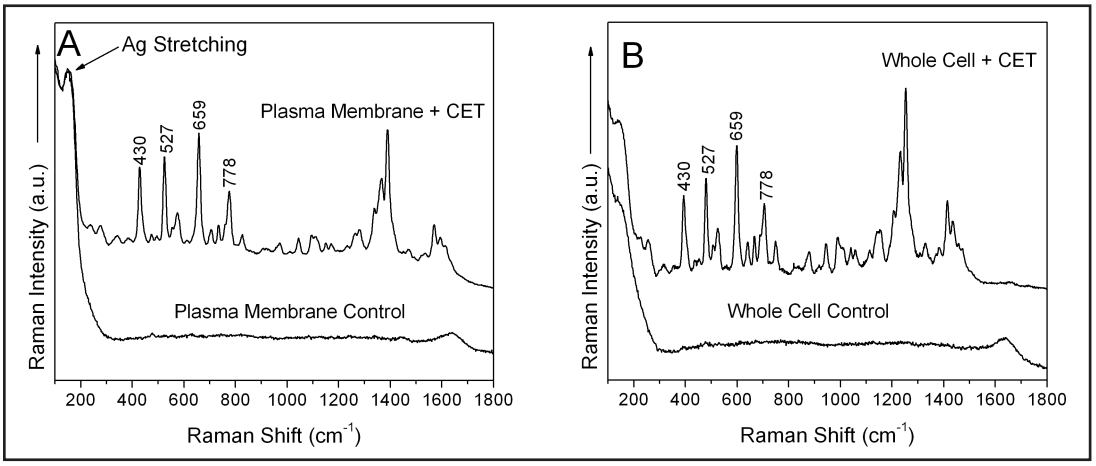

Fig. 5. A) SERS spectra of untreated and CET- treated purified plasma membrane fractions expanded in the fingerprint region. B) SERS spectra of whole cell extracts from HLECs with and without CET exposure done in the presence of CHAPS (see Methods). Spectra are intensity-shifted for comparison purposes.

Table 2. Estimated Concentrations of CET within HLEC Extracts.[a]CET concentrations were determined by accounting for a 1:20 dilution factor within the SERS samples. Values in ( ) are the SD for N = 3 individual measurements

HLEC Extract	Integrated 659 cm^{-1} Intensity (a.u.)	Normalized 659 cm^{-1} Intensity	-Log [CET] SERS Sample	M [CET][a] in Extract	Moles CET/ µg protein
A. Crude Membranes	124,34	1.015	4.87 (26)	2.70 (2) x 10^{-4}	1.68 x 10^{-10}
B. Cytosol	80,65	0.658	6.81 (36)	1.04 (18) x 10^{-6}	5.15 x 10^{-13}
C. Plasma Membrane	110,54	0.902	5.48 (21)	8.19 (37) x 10^{-5}	1.01 x 10^{-10}
D. Whole Cell Extract	48,89	0.399	8.23(44)	1.16 (16) x 10^{-7}	2.78 x 10^{-13}

marker bands were observed in the cytosolic or plasma membrane extracts under regular Raman conditions, consistent with CET concentrations below 10^{-3} M in each sample (Fig. 4).

The SERS spectra of CET-treated cytosolic, and crude and purified plasma membrane fractions exhibited the four distinct marker bands of CET (Fig. 4B, 5), even when using

relatively short acquisition times (3 sec in each). In addition, the extensive biological matrix present in each sample did not appear to affect the intensity of each marker band. This is likely the result of a high degree of affinity between the positively charged iminium nitrogen and the predominantly negatively charged AgNPs in each sample. Previous SERS analyses of molecules of similar structure containing positively charged amino groups (*e.g.*, rhodamine 6G) further corroborate this finding [28]. Total areas for the 659 cm^{-1} peak/sample were normalized, and concentrations were interpolated using the empirical relation derived from the calibration procedure and the dilution factors (Table 2).

The data in Table 2 yield the CET molar concentration (column 5) measured in the 20 fold-diluted cytosol and membrane extracts (column 1). Extracts A and B are from the same experiment, and C and D from different experiments. In A/B HLECs were disintegrated by MPER, and only the insoluble crude membrane material further solubilized with 1% CHAPS. It is evident that on a mol CET μg^{-1} protein basis there was $3x10^{-2}$ more CET in the crude membrane fraction than in the cytosol. Based on the calculated dilution factor of the HLEC cytosol of 41 (see Methods), the $[CET]_i$ in the cytosol is computed as 43 x 10^{-6} M, which is close to the extracellular [CET] 50 x 10^{-6} M. When the crude membranes were subjected to two centrifugation steps (see Methods), the resulting plasma membrane pellet (Table 2 C) exhibited a ~70% reduction in CET consistent with riddance from other particulate material such as endoplasmic reticulum, Golgi and mitochondrial membranes and most likely nuclear material. Still, normalized to protein, most of the CET preferred to lodge within the membranes. For the whole cell extract obtained in the presence of 1% CHAPS to solubilize all membrane material (with exception of a small but distinct CET-positive insoluble pellet), the CET content μg^{-1} protein was within the same order of magnitude, yielding 1.97 x 10^{-11} instead of 2.11 x 10^{-11} CET content μg^{-1} protein, consistent with similar cytosolic concentrations of CET in near equilibrium with the external media.

In conclusion these data suggest that SERS is capable to determine the free cytosolic concentration of monomeric CET, but also shows that a rather large CET membrane pool exists suggesting that the total CET that is associated with the cell probably exceeds diffusion equilibrium.

Discussion

Previously, it was proposed that the QBA CET inhibits NKP by binding to at least one BH1 motif discovered within the NKP's actuator (A) domain, thus, for example constraining the 120° rotation of the A domain and its temporary protection of the high energy aspartate 369-phosphate residue that confers the conformation required for the trapping of the 3 Na^+ ions in an occluded state [10].

The rationale for the present study was to provide proof of concept by establishing the distribution of CET between the cytosol and the crude plasma membrane preparation using a novel technological approach, SERS, with the ultimate goal to identify the compound within the NKP structure. The use of the large signal enhancement of SERS over ordinary Raman spectra gave us the advantage to a) characterize CET based on its four marker bands (Fig. 1), b) identify it in concentrations less than 10^4 orders of magnitude smaller than Raman spectroscopy would have done (Fig. 2A and B) and thus establish a calibration curve (Fig. 3) over five orders of magnitude, and c) identify within cytosol and crude and purified plasma membrane fractions, CET concentrations in the micromolar range (Fig. 4 and 5, Table 2). Therefore, the greater sensitivity of the SERS method coupled to the minimal pre-resonance effects of the 532 nm laser excitation wavelength also easily surpassed by several orders other approaches such as UV-VIS spectrometry, where the limit of detection was around 10^{-4} to 10^{-5} M (c.f. Fig. 1B). Furthermore, these results show extreme promise in the ability of SERS to be used as a sensitive and specific technique for tracking small molecule cellular metabolites with visible absorption resonances, even within crude cellular matrices.

As shown in Table 2, the CET cytosolic concentrations were quite close to that of the bathing medium of 50 μM, raising the question as to whether CET might equilibrate across the plasma membrane, as a positively charged monomer (CET^+) or as pseudo base that does exist at higher pH values [30]. For the sake of the argument, if CET traversed the membrane as CET^+, then, according to the Nernst Equation: $\log [CET^+]_i = \log [CET]_o - E_m/61.5$, the free intracellular CET concentration, $[CET]_i$, should have been 5 fold above equilibrium at 244 μM, assuming a membrane potential, E_m, of - 40 mV typical in epithelial cells, where $[CET]_o$ is the external CET concentration = 50 μM, and 61.5 mV = 2.3 RT/zF at 37 °C with the usual meanings. If we assume that the cytosolic and membrane CET content add up altogether within one cellular compartment, the total $[CET]_i$ should be 267 μM, a value that is close to that predicted from the Nernst equation. Thus it is not improbable that indeed CET traverses as CET^+ rapidly equilibrating perhaps through cationic channels that are capable to accommodate the 348 dalton compact benzo-phenanthridine ring. In this context, it is of interest that epithelial cells have at least two isoforms of organic cation channels, OCT1 and OCT2 [32], and their presence is currently evaluated in terms of their capability to transport positively charged QBAs. Moreover, it has also been shown that transport through epithelial OCTs plays a pivotal role in the targeting of positively charged QBAs to the plasma membrane. The time-dependent fate of CET cellular distribution will be further investigated to shed light on this issue.

Finally, based on the calculated number of 10^{13} CET molecules μg^{-1} crude membrane protein and assuming that at least 10% of the membrane protein is NKP with a molecular weight of 10^5 Daltons, one can compute a ratio of CET/NKP of about 100, a number still far exceeding the expected ratio of not more than 2 based on the putative presence of two BH1 motifs/NKP with solvent accessibility for CET. Experiments ongoing with affinity purified NKP using mouse-anti human α1 NKP subunit antibody either from plasma membrane-free cytosolic or from purified membrane fractions suggest a CET/NKP ratio of <1. Differences currently addressed may be due to a) insufficient washing of the crude membrane particles releasing all trapped CET only in the presence of CHAPS, b) the tendency of CET to partition and lodge within the structurally not unrelated cholesterol component of the membrane bilayer, c) charge interactions with negatively charged lipids and proteins with neuraminic acid residues, d) absorption to residual nuclear material in particular in the crude membrane fraction, e) trapping of the alkaloids within putative organic cation channels, and last but not least interferences of solvents and CET-binding macromolecules with AgNP augmentation of the electromagnetic signals, i.e. SERS-based nano-sensing.

Conclusions

The NKP is a target of QBAs and recent findings implicate at least two BH1-like motifs within the crystal structure of the transporter to which CET, a BH3-mimetic, might bind and inhibit function [10]. Using a novel approach, SERS-based nano-sensing, the distribution of the QBA CET between the plasma membrane and the cytosolic extracts of HLECs was studied. The data suggest that CET most likely travels as the charged monomeric CET^+, because already the free cytosolic CET concentration approached the external CET concentration, and the plasma membrane contained CET exceeding that of the cytosol on a protein basis by more than 2 orders of magnitude.

Conflict of Interests

None

Acknowledgments

Part of this work was presented at the 2013 Lake Cumberland Biological Transport Meeting, Ky. Dr. Sizemore highly acknowledges the WSU start-up fund.

References

1 Weiss D, Baumert A, Vogel M, Roos W: Sanguinarine reductase, a key enzyme of benzophenanthridine detoxification. Plant Cell Environ 2006;29:291-302.
2 Burrows GE, Tyrls RJ: Toxic plants of north america, ed 2nd. John Wiley & Sons, Inc, 2013.
3 Herbert J, Augereau J, Gleye J, Maffrand J: Cheleryhtrine is a potent and specific inhibitor of protein kinase c. Biochem Biophys Res Commun 1990;172:993-999.
4 Chmura SJ, Dolan ME, Cha A, Mauceri HJ, Kufe DW, Weichselbaum RR: In vitro and in vivo activity of protein kinase c inhibitor chelerythrine chloride induces tumor cell toxicity and growth delay in vivo. Clin Cancer Res 2000;6:737-742.
5 Courage C, Budworth J, Gescher A: Comparison of ability of protein kinase c inhibitors to arrest cell growth and to alter cellular protein kinase c localisation. British J Cancer 1995;71:697-704.
6 Kaminskyy V, Lin KW, Filyak Y, Stoika R: Differential effect of sanguinarine, chelerythrine and chelidonine on DNA damage and cell viability in primary mouse spleen cells and mouse leukemic cells. Cell Biol Int 2008;32:271-277.
7 Chan S-L, Lee MC, Tan KO, Yang L-K, Lee ASY, Flotow H, Fu NY, Butler MS, Soejarto DD, Buss AD, Yu VC: Identification of chelerythrine as an inhibitor of bclxl function. J Biol Chem2003;278:20453-20456.
8 Chan S-L, Yu VC: Proteins of the bcl-2 family in apoptosis signaling: From mechanistic insights to therapeutic opportunities. Clin ExpPharmacol Physiol 2004;31:119-128.
9 Wan KF, Chan S-L, Sukumaran SK, Lee M-C, Yu VC: Chelerythrine induces apoptosis through a bax/bak-independent mitochondrial mechanism. J Biol Chem 2008;283:8423-8433.
10 Lauf PK, Heiny J, Meller J, Lepera MA, Koikov L, Alter GM, Brown TL, Adragna NC: Canonical bcl-2 motifs of the Na^+/K^+ pump revealed by the BH 3 mimetic chelerythrine. Early signal transducers of apoptosis? Cell Physiol Biochem 2013;31:257-276.
11 Cala P, Norby J, Tosteson D: Effects of the plant alkaloid sanguinarine on cation transport by human red blood cells and lipid bilayer membranes. J Membr Biol 1982;64:23-31.
12 Cohen HG, Seifen EE, Straub KD, Tiefenback C, Stermitz FR: Structural specificity of the nak-atpase inhibition by sanguinarine, an isoquinoline benzophenanthridine alkaloid. Biochem Pharmacol 1978;27:2555-2558.
13 Janovska M, Kubala M, Suimanek V, Ulrichova J: Interaction of sanguinarine and its dihydroderivative with the Na^+/K^+-atpase. Complex view on the old problem. Toxicol Lett 2010;196:56-59.
14 Meyerson LR, McMurtrey KD, Davis VE: Isoquinoline alkaloids. Neurochem Res 1978;3:239- 257.
15 Seifen E, Adams R, Riemer R: Sanguinarine: A positive inotropic alkaloid which inhibits cardiac Na^+/K^+-atpase. Eur J Pharmacol 1979;60:373-377.
16 Straub KD, Carver P: Sanguinarine, inhibitor of Na^+/K^+-dependent atp'ase. Biochem Biophys Res Comm 1975;62:913-922.
17 Straub KD, Seifen E, Adams JM, Bissett JK, Kane JJ, Murphy ML, Doherty JE: Cardiac effects of sanguinaria alkaloid: A new digitalis antagonist with positive ionotropic and antiarrhythmic actions. Circulation 1977;56:III-129.
18 Janovska M, Kubala M, Simaek V, Ulrichova J: Fluorescence of sanguinarine: Spectral changes on interaction with amino acids. Phys Chem Chem Phys 2010;12:11335-11341.
19 Slaninova I, Slanina J, Taborska E: Quaternary benzo[c]phenanthridine alkaloids-novel cell permeamt and red fluorescing DNA probes. Cytometry 2007;71:700-708.
20 Bonham AJ, Braun G, Pavel I, Moskovitz M, Reich NO: Detection of sequence-specific protein-DNA interactions via surface-enhanced raman scattering. J Am Chem Society 2007;129:14572-14573.

21 Pavel I, McCarney E, Elkahaled A, Morrill AK, Plaxco K, Moskovits M: Label-free sers detection of small proteins modified to act as bifunctional linkers. J Phys Chem 2008;C112:4880-4883.
22 Lauf PK, Di Fulvio M, Srivastava V, Sharma N, Adragna NC: Kcc2a expression in a human fetal lens epithelial cell line. Cell Physiol Biochem 2012;29:303-312.
23 Lauf PK, Misri S, Chimote AA, Adragna NC: Apparent intermediate K^+ conductance channel hyposmotic activation in human lens epithelial cells. Am J Physiol - Cell Physiol 2008;294:C820-C832.
24 Adragna NC: Cation transport in vascular endothelial cells and aging. J Memb Biol 1991;124:285-291.
25 Creighton JA, Blatchford CG, Grant AM: Plasma resonance enhancement of raman scattering by pyridine absorbed on silver or gold sol particles of size comparable to the excitation wavelength. J Chem Soc, Faraday Trans 1979;275:790-798.
26 Trefry JC, Monahan JL, Markopolous MM, Arnold ZS, Wooley DP, Pavel IE: Size selection and concentration of silver nanoparticles by tangential flow ultrafiltration for sers-based detection. J Am Chem Soc 2010;132:10970-10972.
27 Stamplecoskie KG, Scaiano JC, Tiwari VS, Anis H: Optimal size of silver nanoparticles for surface-enhanced raman spectroscopy. J Phys Chem 2011;C115:1403-1409.
28 Hildebrant P, Stockburger M: Surface-enhanced resonance raman spectrocopy of rhodamine 6g absorbed on colloidal silver. J Phys Chem 1984;88:5935-5944.
29 Dollish FR, Fateley WG, Bentley FF: Characteristic raman frequencies of organic compounds. John Wiley & Sons, Inc., 1974.
30 Dostal J, Taborska E, Slavik J, Potacek M, de Hoffmann E: Structure of chelerythrine base. J Nat Prod 1995;58:723-729.
31 Lin-Vien D, Colthup NB, Fateley WG, Grasselli G: The handbook of infrared and raman characteristics., Academic Press, Inc., 1991.
32 Koepsell H: Polyspecific organic cation transporters and their biomedical relevance in kidney. Cur Opin Nephrol Hypertens 2013;22:533-538.